

pubs.acs.org/journal/abseba Article

# Heavy Metal Exposure Leads to Rapid Changes in Cellular Biophysical Properties

Peiran Zhu, → Jamar Hawkins, → Will Hamilton Linthicum, Menglin Wang, Ningwei Li, Nanjia Zhou, Qi Wen, Alicia Timme-Laragy, Xiaofei Song,\* and Yubing Sun\*



Cite This: ACS Biomater. Sci. Eng. 2020, 6, 1965–1976



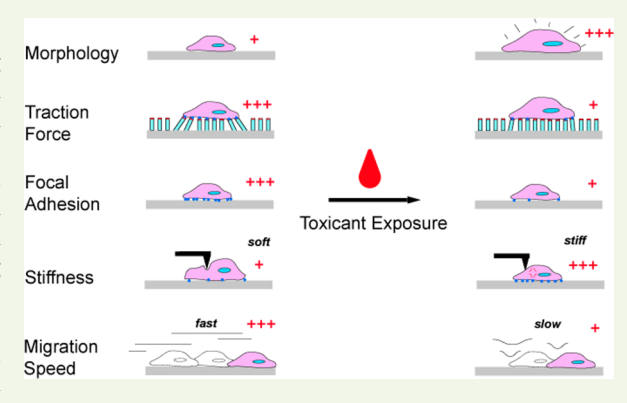
**ACCESS** 

III Metrics & More

Article Recommendations

s Supporting Information

ABSTRACT: Biophysical properties of cells, such as cell mechanics, cell shape, and cell migration, are emerging hallmarks for characterizing various cell functions. Conversely, disruptions to these biophysical properties may be used as reliable indicators of disruptions to cell homeostasis, such as in the case of chemical-induced toxicity. In this study, we demonstrate that treatment of lead(II) nitrate and cadmium nitrate leads to dosage-dependent changes in a collection of biophysical properties, including cellular traction forces, focal adhesions, mechanical stiffness, cell shape, migration speed, permeability, and wound-healing efficacy in mammalian cells. As those changes appear within a few hours after the treatment with a trace amount of lead/cadmium, our results highlight the promise of using biophysical properties to screen environmental chemicals to identify potential toxicants and establish dose response curves. Our systematic and quantitative characterization



of the rapid changes in cytoskeletal structure and cell functions upon heavy metal treatment may inspire new research on the mechanisms of toxicity.

**KEYWORDS:** biophysics, environmental pollutants, lead, cell traction force, AFM, cell stiffness, focal adhesion, MTT, micropattern, cell morphology, permeability, wound healing

## **■** INTRODUCTION

Cellular-scale biophysical properties, such as cell mechanics, cell shape, and cell migration, are emerging biomarkers for cell characterization, as these properties are often closely associated with various status changes of cells including differentiation, metastasis, and aging. 1-4 For instance, cell shape and traction forces regulate the neuronal differentiation potential of human pluripotent stem cells,<sup>5</sup> and cell stiffness has been reported to correlate with cancer cell motility and invasion.<sup>6,7</sup> Recently, Wirtz and co-workers thoroughly investigated the biophysical properties of primary human dermal fibroblasts from individuals between 2 and 96 years of age and achieved a more accurate cellular age prediction than conventional biomolecular markers by characterizing several cellular biophysical features.8 Despite the importance of biophysical properties for cell physiology studies, as well as the advantages in more affordable sample preparation and less expensive labeling,<sup>9</sup> it is still unclear how cellular biophysical properties change in response to toxicants and whether this may be a useful assessment in the field of toxicology.

Toxicant-induced cellular level dysfunctions can potentially result in diseases including nephropathies, hepatopathies, and cancers. For example, exposure to environmental toxicants such as lead and cadmium can result in the

progressive loss of kidney function. Naturally, toxicant detection has become a critical factor in the diagnosis and treatment of chronic kidney diseases. 13,14 To understand the relative potencies of various toxicants, in vitro biochemical assays such as cell viability colorimetric assays and live/dead assays are routinely used to evaluate the cytotoxicity of environmental toxicants.<sup>15</sup> Though cell viability assays can characterize the biochemical responses of cells to toxicants, there remains the unmet need of characterizing the biophysical responses to further elucidate how organs and tissues are affected. Emerging results demonstrated that sublethal concentrations of heavy metal ions<sup>16–18</sup> and nanoparticles<sup>19–21</sup> could cause drastic changes in cytoskeletal structures which in turn impair cell adhesion and migration. However, the effects of toxicants on biomechanical features such as cell stiffness and cell contractility have not yet been systematically characterized.

Received: October 28, 2019 Accepted: March 13, 2020 Published: March 13, 2020





In this work, we reveal the characteristic changes in cell biophysical properties in the presence of common two environmental toxicants: lead and cadmium. At the singlecell level, the traction force, focal adhesions, cell morphology, migration speed, and stiffness were measured for single cells under varying concentrations of lead(II) nitrate. Next, we investigated the effect of lead on the biophysical properties of a cell monolayer, where the monolayer permeability and woundhealing speed were measured. Our results demonstrate changes in various biophysical properties attributed to even very low (10 µM) concentrations of lead. In contrast, no significant difference between control and lead-treated groups can be detected using lactate dehydrogenase (LDH) and methylthiazolyl-tetrazolium (MTT) assays at this level. Notably, previous studies also reported that the lead cytotoxicity and oxidative stress in mammalian cells were only detectable using various assays at a relatively high concentration (>50  $\mu$ M) after at least 24 h of exposure. 22,23 We further demonstrate that another heavy metal, cadmium, could also lead to cellular biophysical properties changes but in a different manner compared to lead. Therefore, biophysical phenotyping may present a new opportunity to facilitate the understanding of the effects of environmental toxicants.

# ■ MATERIALS AND METHODS

Chemicals and Exposure Diagram. Stock solutions of 1 M lead(II) nitrate (CAS 10099-74-8, Fisher Scientific, Waltham, MA) or 0.5 M cadmium nitrate (CAS 7697-37-2, Millipore Sigma, Burlington, MA) were run through a 0.22  $\mu$ m filter (Millipore Sigma, Burlington, MA). After filtration, the stock solutions were diluted with ultrapure water and stored at room temperature. The toxicant solution was further diluted with cell culture medium to specific concentrations: 0 (control), 0.01, 0.1, and 1 mM for lead(II) nitrate and 0 (control), 0.005, 0.05 mM for cadmium nitrate. After at least 12 h of cell seeding, cell culture medium was aspirated, and toxicant-enriched cell culture medium was added. Cells were analyzed after either 2, 4, or 24 h of toxicant treatment

Cell Line and Culture. The Madin Darby canine kidney cells (MDCK NBL-2), a widely used mammalian epithelial model, were grown in Dulbecco's modified eagle medium (DMEM; 11960-051, Life Technologies) supplemented by 10% FBS (Sigma-Aldrich) with 1% penicillin/streptomycin (Gibco), 1% GlutaMAX (100X, 35050-061, Gibco), and 1% sodium pyruvate (100 mM, 11360-070, Gibco). Cells were cultured at 37 °C and with 5% CO<sub>2</sub>. Media were changed every 3 days, and cells were passaged when they were nearly 90% confluent using 0.25% trypsin-EDTA (Gibco). The rat embryonic fibroblasts (REF-52) were grown in Dulbecco's modified eagle medium (DMEM; 11960-051, Life Technologies) supplemented by 10% fetal bovine serum (FBS; Sigma-Aldrich) with 1% penicillin/ streptomycin (Gibco), 1% GlutaMAX (100X, 35050-061, Gibco), and 1% MEM nonessential amino acids (MEM NEAA; 100X, 11140-050, Gibco). Cells were cultured at 37 °C and with 5% CO<sub>2</sub>. Media were changed every 3 days, and cells were passaged when they were nearly 90% confluent using 0.25% trypsin-EDTA (Gibco).

**Methyl-thiazolyl-tetrazolium (MTT) Assay.** The cytotoxicity of the lead was evaluated using an MTT assay. One hundred microliters of cells (including 5000 cells) was transferred to each well of a 96-well plate and allowed to adhere and recover for 24 h. Then the cells were treated with the desired concentration of lead nitrate and cultured for 2, 4, 12, and 24 h. Cells were washed using PBS prior to treatment with MTT. Subsequently, 100  $\mu$ L of MTT (5 mg/mL in medium) was added in each well and incubated for 4 h. The media were removed, and the dyes dissolved in 100  $\mu$ L of DMSO were added. After the samples were shaken for 30 min, the absorbance was measured at  $\lambda = 570$  nm in Cytation 3 Cell Imaging Multi-Mode Reader (BioTek).

**Lactate Dehydrogenase (LDH) Assay.** The cytotoxicity of the lead was also evaluated using a Pierce LDH cytotoxicity assay kit (Thermo Fisher Scientific, Waltham, MA). To prevent noise from LDH in FBS, the percentage of FBS in the medium was reduced from 10% and 5%. One hundred microliters of cells (5000 REF/15 000 MDCK) was transferred to 18 wells of a 96-well plate and allowed to recover for 12 h. The cells were then treated with the desired concentration of lead (either 0, 0.01, 0.1, or 1 mM) and incubated for 2, 4, or 24 h. After incubation, 50  $\mu$ L of the supernatant from each well was transferred to a new well-plate and mixed with 50  $\mu$ L of LDH reaction mixture. The resulting mixture was incubated for an additional 30 min protected from light. Finally, the stop solution was added to each well, and the absorbance at 490 and 680 nm was measured using a Cytation 3 Cell Imaging Multi-Mode Reader (BioTek). Assays were performed with both MDCK and REF cells.

Microcontact Printing. Fixed patterns were generated using soft lithography and microcontact printing techniques, as described previously. A,25 Briefly, patterned PDMS stamps were molded from negative SU8 molds that were fabricated using photolithography. Round glass 18 mm diameter coverslips (Fisher Scientific) were spincoated (Spin Coater; Laurell Technologies) with a thin layer of PDMS prepolymer containing PDMS base monomers and curing agents (10:1 w/w; Sylgard 184, Dow-Corning) before the PDMS layer was thermally cured by baking at 110 °C for at least 24 h. In parallel, PDMS stamps were soaked in fibronectin solution (50 µg· ml<sup>-1</sup> in sterile, deionized water) for 1 h. Excess fibronectin was then washed away by DI water, and the stamps were dried with a stream of N2. Fibronectin-coated stamps were gently placed on the top of the flat PDMS substrates, following treatment with UV ozone for 7 min. The stamps were pressed gently to facilitate the transfer of fibronectin to coverslips. Protein adsorption to all PDMS surfaces not coated with fibronectin was prevented by immersing coverslips in 0.2% Pluronics F127 NF solution (Sigma) for 30 min. Coverslips were rinsed with PBS and transferred to standard 12-well tissue culture plates for seeding cells.

**Live/Dead Cell Viability Assay.** Cells were labeled with 4  $\mu$ M EthD-1 and 2  $\mu$ M calcein-AM according to the manufacturer's instructions.

**Traction Force Microscopy.** Traction force was analyzed using PDMS micropost arrays (PMAs) as described previously <sup>4,26</sup> (Figure S1). Briefly, PMAs were first functionalized for cell attachment using microcontact printing to coat micropost top surfaces with fibronectin. PMAs were labeled with DiI (5  $\mu$ g mL<sup>-1</sup>; Life Technologies) in distilled water for 1 h. After microcontact printing, protein adsorption to all PDMS surfaces not coated with fibronectin was prevented by incubating in 0.2% Pluronics F127 NF solution (Sigma) for 30 min. Images of micropost tops were recorded using a 40× objective (Leica DMi8). All images were analyzed using a custom-developed MATLAB program (MathWorks), as described previously, <sup>27</sup> to obtain traction force maps associated with each image.

**Vinculin Staining.** Cells were incubated in an ice-cold cytoskeleton buffer (50 mM NaCl, 150 mM sucrose, 3 mM MgCl<sub>2</sub>, 1 mg/mL aprotinin, 1 mg/mL leupeptin, 1 mg/mL pepstatin, and 2 mM PMSF) for 1 min, followed by 1 min in the cytoskeleton buffer supplemented with 0.5% Triton X-100. After that, the mouse antivinculin primary antibody (Sigma-Aldrich, St. Louis, MO) was used and detected by the goat-antimouse Alexa-488 secondary antibody.

**F-Actin Staining.** Cells were fixed with 4% paraformaldehyde before being labeled with Phalloidin (A12379, Alexa Fluor 488 Phalloidin, 1:40) according to the manufacturer's instructions.

Cell Motility. Cells were seeded at a low density (3000 cells/mL) onto 35 mm tissue-culture Petri dishes (Corning) and allowed to adhere and recover for 12 h. After lead treatment, cells were mounted on a Leica DMi8 microscope equipped with a monochrome charge-coupled device (CCD) camera and an environment control to maintain the physiological temperature, CO<sub>2</sub>, and humidity (H301-K-FRAME, OKOLAB). Phase-contrast images were taken every 5 min for 2, 4, and 10 h. The migration speed and trajectory were analyzed by CellTracker.<sup>28</sup>

Cell Stiffness Measurement. MDCK cells were seeded at 15-20% confluency onto untreated polystyrene dishes in lead-free media to enable sufficient adhesion to the culture dish before lead treatment. After 12 h, the culture media were changed in each dish to one of the four lead concentrations (0, 0.01, 0.1, 1 mM). The cells continued to incubate for 24 h before being measured for stiffness using an MFP-3D-BIO atomic force microscope (Asylum Research). DNP cantilevers (Bruker) with nominal spring constant 0.06 N/m were individually calibrated for spring constant and inverse optical lever sensitivity (invOLs) through thermal tuning and linear force curvefitting on the glass in liquid, respectively. Cells with minimal contact with neighboring cells were selected for measurement to minimize cell-to-cell interactions affecting cell mechanical behavior. Each force curve was characterized by a 2  $\mu$ m/s indentation until a trigger force of 1 nN on the cantilever was achieved. Three locations on each cell in the perinuclear region were measured and averaged. No more than 30 min was spent measuring any individual dish to minimize environmental artifacts.

Stiffness values (*E*) were determined from the force curve measurements through a custom MATLAB code that automatically selects the initial contact point and fits the force curve over a 400 nm indentation range that satisfies the Hertz model:

$$E = \frac{kd\pi(1 - \nu^2)}{2\Delta^2 \tan \phi}$$

where k is the spring constant of the cantilever, d is the deflection of the cantilever,  $\nu$  is the Poisson's ratio (assumed as an incompressible material  $\nu=0.5$ ),  $\Delta i$  is the indentation depth of the sample, and  $\Phi$  is the half angle of the conical cantilever tip  $(17.5^{\circ})^{29,30}$ 

Scratch Wound Healing. MDCK cells were seeded on a 35 mm tissue-culture Petri dishes (Corning) with a high density (1  $\times$   $10^6$  cells/mL) and cultured to confluence for 24 h. Four vertical scratches were made in the confluent monolayer of cells using a P1000 micropipette tip (Fisher Scientific, Catalog number, 02-707-402). Next, cells were washed once with PBS before being treated with lead and then mounted on a Leica DMi8 microscope equipped with a monochrome charge-coupled device (CCD) camera and an environment control to maintain the physiological temperature,  $\rm CO_2$ , and humidity (H301-K-FRAME, OKOLAB). Phase-contrast images were taken every 6 h.

**Permeability Assay.** MDCK cells were seeded at a high density of  $1 \times 10^6$  cells/mL on Transwell Permeable Supports (6.5 mm insert, 24 well plate, 0.4  $\mu$ m polyester membrane, Costar) and cultured to a confluent monolayer for 48 h. Cells then were treated with the desired concentration of lead for 2, 4, and 24 h. The volume of medium for the inside of transwell insert was 0.1 and 0.6 mL for plate well. Subsequently, cells were washed three times with PBS before adding Fluorescein isothiocyanate (FITC)-Dextran (wt = 40 000, dissolved to 50 mg/mL, 0.1 mL FITC-Dextran for apical well, 0.6 mL medium without FITC-Dextran for basolateral well). Cells were incubated for 1 h, and 0.1 mL of medium was taken from the basolateral chamber. Then, the medium was transferred to a 96-well plate, and fluorescence ( $\lambda_{\rm ex}$  = 488 nm,  $\lambda_{\rm em}$  = 520 nm) was measured in the plate reader described above.

Transepithelial Electrical Resistance (TEER Test). MDCK cells were seeded at a density of 200 000 cells/mL on Transwell Permeable Supports (6.5 mm insert, 24 well plate, 0.4  $\mu$ m polyester membrane, Costar) and cultured to a confluent monolayer for 4–6 days. The volume of medium for the inside of transwell insert was 0.1 and 0.6 mL for basolateral well. The medium was changed every 48 h in both the apical and basolateral wells. After 4 days, TEER was measured using an EVOM epithelial voltmeter (World Precision Instruments, Sarasota, FL) with manual chopsticks to determine if monolayer was confluent. A TEER value between 500 and 550  $\Omega$ ·cm² was considered fully confluent, as the TEER values for all wells stabilized within that range. Cells then were treated with the desired concentration of lead, and the TEER value of each transwell was recorded at 2, 4, and 24 h.

**Image Analysis.** Phase and fluorescence images were recorded using an inverted epifluorescence microscope (Leica DMi8; Leica

Microsystems) equipped with a monochrome charge-coupled device (CCD) camera. ImageJ (NIH, Bethesda, MD) was used for the measurement of the area of cells.

**Statistics.** Statistical analysis was performed using GraphPad Prism. For statistical comparations between two data sets, P-values were calculated using the student *t* test function. For statistical comparations between three or more data sets, P-values were calculated using the one-way ANOVA with Tukey posthoc analysis.

### RESULTS

Assessing the Cytotoxicity of Lead by Conventional Cell Viability Assays. Colorimetric cell viability assays including LDH and MTT have been used to quantify cell killing by toxicants.<sup>31</sup> Therein, the reduction of MTT to formazan depends on mitochondrial flavin containing enzymes and NAD(P)H in intact cells. The MTT assay has been utilized to assess cell viability, proliferation, and cytotoxicity.<sup>32</sup> Therefore, we first examined the killing of MDCK cells by lead using the MTT assay. With 24 h exposure to a series of increasing concentrations (0.01, 0.1, 1.0 mM) of lead, MDCK cells showed decreased viability compared to the control. However, no statistically significant concentration dependence was observed for the range within 0.01–1.0 mM (Figure 1a).

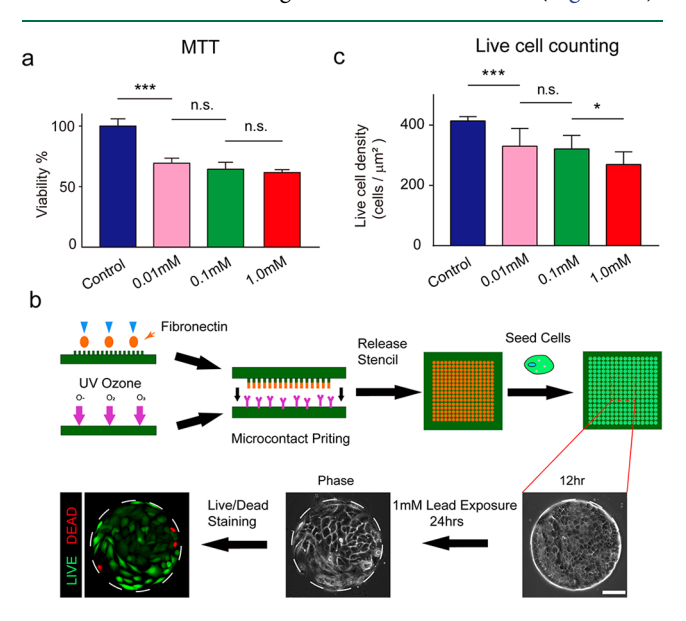


**Figure 1.** Live/dead assay and MTT assay for characterizing cell viability. (a) Bar plot presenting the cell viability compared with the control group. (b) Schematic diagram presenting the procedures of seeding cells on micropatterns and the representative immunofluor-escence and phase images showing the live/dead staining. Scale bar,  $100~\mu m$ . (c) Bar plot showing the live-cells density of each pattern after lead exposure.  $n_{\rm colony}=25$ . MDCK cells were exposed to lead nitrate with 0, 0.01, 0.1, 1 mM for 24 h. Data represent mean and standard deviation from at least three independent experiments. \*, P < 0.05, \*\*\*, P < 0.001, n.s., P > 0.05.

We then performed the LDH assay which detects the release of LDH from damaged cells with high sensitivity. As shown in Figure S2, only the highest lead concentration (1 mM) led to a significant increase of LDH level in MDCK cells. As an alternative to these colorimetric assays which may suffer from unexpected aritifacts, we then directly counted the percentage of dead cells induced by lead exposure. Using microcontact printing, we generated an array of adhesive islands for MDCK cell culturing (Figure 1b) from which we

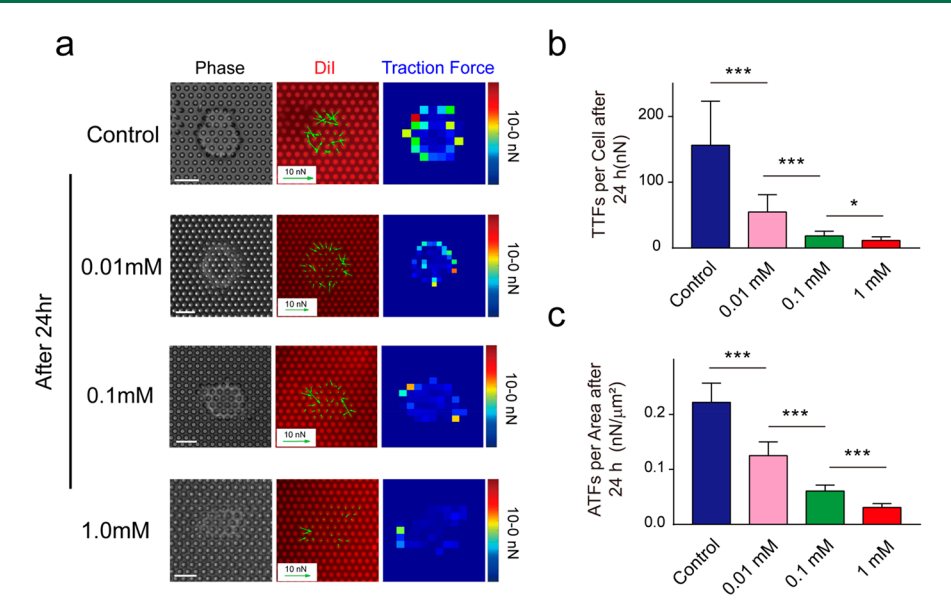


**Figure 2.** Lead induced a significant reduction of cell traction forces. (a) Left: Representative phase images showing a MDCK cell exposed to lead on PMA substrates after 24 h. Middle: Microposts labeled with DiI (red) and vector maps of traction forces (green). Right: Colorimetric map showing traction forces. Scale bar,  $10 \, \mu \text{m}$ . (b-c) Bar plots comparing the TTFs (b) and ATFs (c) after 24 h. MDCK cells were exposed to lead nitrate with 0, 0.01, 0.1, 1 mM for 24 h. Data represent mean and standard deviation from at least three independent experiments. \*, P < 0.05, \*\*\*, P < 0.001. n > 25 cells in each condition.

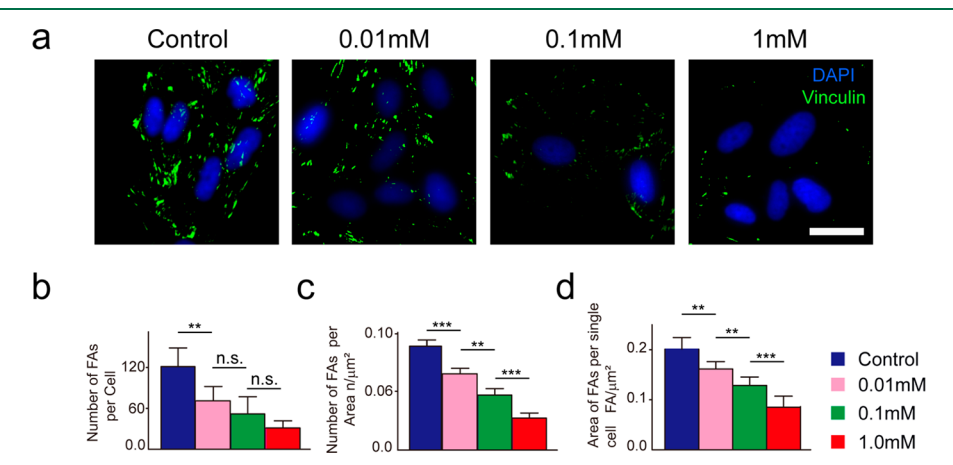


**Figure 3.** Focal adhesions of MDCK cells decreased after exposure to lead. (a) Representative immunofluorescence images showing focal adhesion distributions in MDCK cells for four experimental groups (control, 0.01, 0.1, and 1 mM). Scale bar, 25  $\mu$ m. (b–d) Bar plots presenting the number of FA per cell (b), the number of FA per area (c), and area of FA per single cell (d). MDCK cells were exposed to lead nitrate with 0, 0.01, 0.1, 1 mM for 24 h. Data represent mean and standard deviation from at least three independent experiments. \*\*, P < 0.01, \*\*\*, P < 0.001, n.s., P > 0.05. n > 25 cells in each condition.

can accurately count the number of dead cells on each pattern after staining the cells using the live/dead assay (see Materials and Methods). Results from the live/dead assay presented a similar trend as those from the MTT assay (Figure 1c). While a significant difference in cell viability was observed between 0.1 and 1 mM of lead treatment, the live/dead assay still failed to distinguish the difference in cell viability between lead concentrations of 0.01 and 0.1 mM.

Single-Cell Biophysical Phenotyping of the Lead Cytotoxicity. We next investigated whether single-cell biophysical properties including cellular traction force, focal adhesion, motility, cell shape, and mechanical stiffness<sup>34</sup> change in response to lead. Traction forces exerted by cells to underlying matrices are essential for cellular functions including cell motility, signal transduction, and extracellular matrix remodeling.<sup>8,35,36</sup> To measure cell traction forces, we

cultured MDCK cells on polydimethylsiloxane (PDMS) micropost arrays (PMAs). We found that after exposing cells to an increasing concentration of lead (0, 0.01, 0.1, and 1.0 mM) for 24 h, total traction forces (TTFs) of these cells decreased from 156.4 to 54.9, 18.5, and 11.63 nN/cell, respectively, and average traction forces per area (ATFs) decreased from 0.22 to 0.13, 0.06, and 0.03 nN/ $\mu$ m², respectively (Figure 2a–c). In contrast to MTT, LDH, and live/dead assays, significant statistical differences were found between all lead concentrations tested (Figure 2b–c). Thus, we conclude that lead(II) nitrate decreases cell traction force in a dose-dependent manner and that cell contractility has a high sensitivity to lead(II) nitrate.

The size and distribution of focal adhesion (FA) complexes strongly correlate with traction forces and cell adhesion strength.<sup>37</sup> Thus, we next stained MDCK cells exposed to

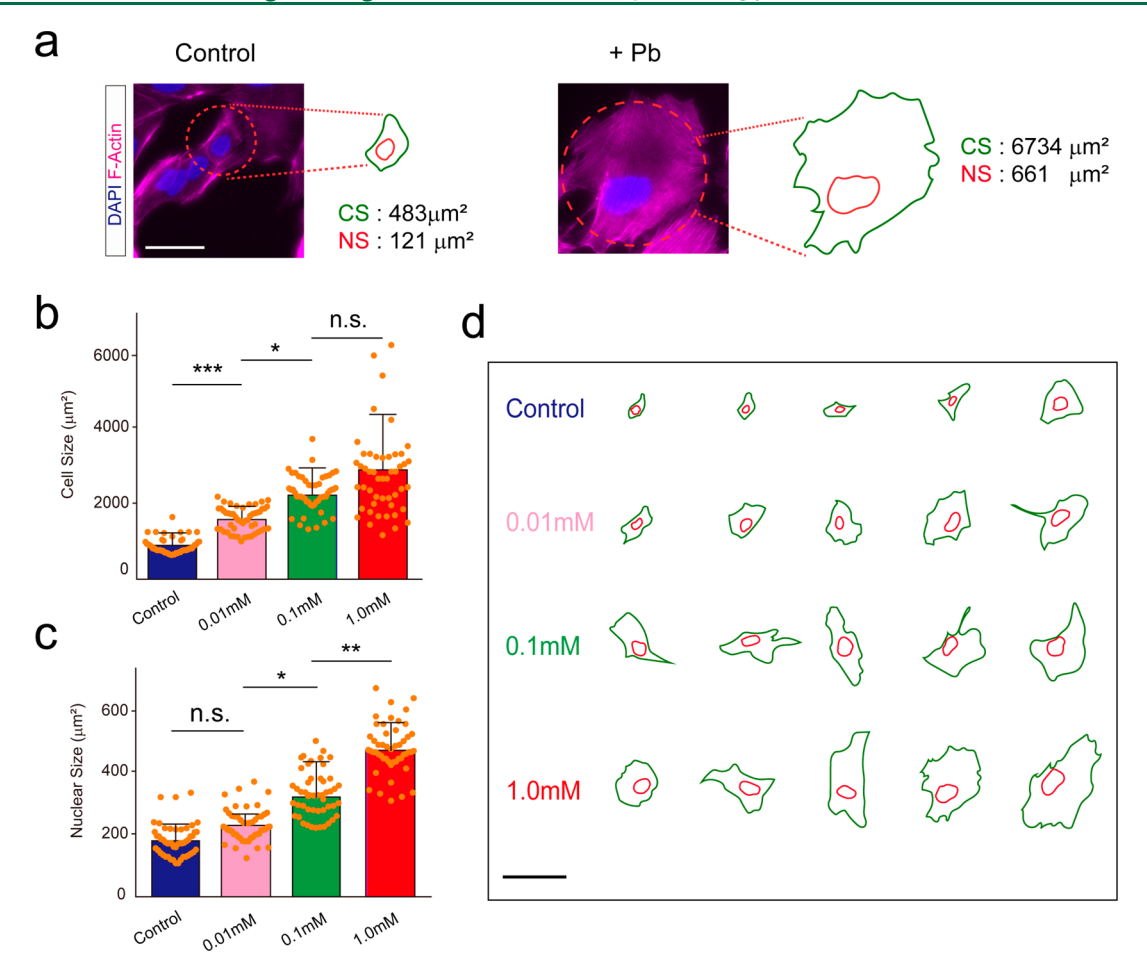


**Figure 4.** Lead-induced increases of cellular and nuclear sizes. (a). Representative fluorescence images showing an untreated MDCK cell (left) and an MDCK cell exposed to 1 mM lead (right). Cells were fixed and stained for F-actin (Phalloidin, pink), nuclei (DAPI, blue). Scale bar, 25 μm. (b-c) Bar plots indicating the cell size (b) and nuclei size (c) after lead exposure. (d) Outlines of the whole cell and cell nuclei of representative cells treated with 0, 0.01, 0.1, and 1.0 mM lead. Scale bar 100 μm. MDCK cells were exposed to lead nitrate with 0, 0.01, 0.1, 1 mM for 24 h. Data represent mean  $\pm$  standard deviation from at least three independent experiments. \*, P < 0.05, \*\*, P < 0.01, \*\*\*, P < 0.001, n.s., P > 0.05. n > 50 cells in each condition.

varying concentrations of the lead with vinculin, an FA protein mediating the force transmission between the cytoskeleton and extracellular matrices—integrin complexes<sup>37,38</sup> (Figure 3a). Consistent with the traction force measurement results, we found that vinculin-expressing FAs drastically declined in the cells exposed to increasing concentration of lead in a dosage-dependent manner. Specifically, the number of FAs per cell and per area (Figure 3b–c) and the total area of FAs per single cell (Figure 3d) all decreased as a function of lead dosage, indicating that the adhesion strength might be attenuated due to the lead treatment. Similar to traction forces, both numbers of FAs per area and the total area of FAs per cell are sufficient to distinguish control and the lead-treated group at the lowest concentration (0.01 mM).

It is known that heavy metal toxicants can disrupt cell growth.<sup>39</sup> Thus, we next investigated cell and nuclear shape changes, both of which are essential mediators of cell functions,<sup>26,40</sup> by F-actin (Phalloidin) and DAPI stains (Figure 4a, Figure S3). We found that both nuclear size and cell spreading area increased upon the lead treatment, depending on the concentration of lead (Figure 4b–c). Changes in the cell and nuclear shapes can also be seen qualitatively from the outline of several representative cells and their nuclei (Figure 4d). Interestingly, although cell and nuclear areas are not as

sensitive as traction forces or FAs, it appears that these two properties have stronger correlations with the concentration of lead, as reflected by larger Pearson correlation coefficients (r = 0.82 for cell area and r = 0.93 for nuclear area), compared with r = -0.78 for FAs r = -0.68 for traction forces.

As cell migration requires the proper function of actomyosin networks, <sup>41</sup> we next utilized live-cell imaging to monitor the migration of single MDCK cells and analyzed the migration trajectories by CellTracker. <sup>28</sup> Quantification results indicated a significant decline of both cell speed and explored distance in lead-treated groups (Figure 5a–c). We also found that the average cell migration speed decreased within the first 4 h after lead treatment (Figure 5b), in contrast to traction forces, FAs, and cell/nuclear shape, which took at least 24 h to show a significant difference between control and treated groups.

Another biophysical property, mechanical stiffness, plays a vital role in cell growth, motility, and tissue homeostasis. Additionally, changes in cell stiffness sometimes denote an abnormality of cell physiology. Hence, we next conducted measurement of cell stiffness by atomic force microscopy (AFM) in control and lead-treated MDCK cells (Figure 6a–c). We observed a significant dosage-dependent increase in cell stiffness, which might originate from the alteration of the cytoskeleton networks of intermediate filaments and associated

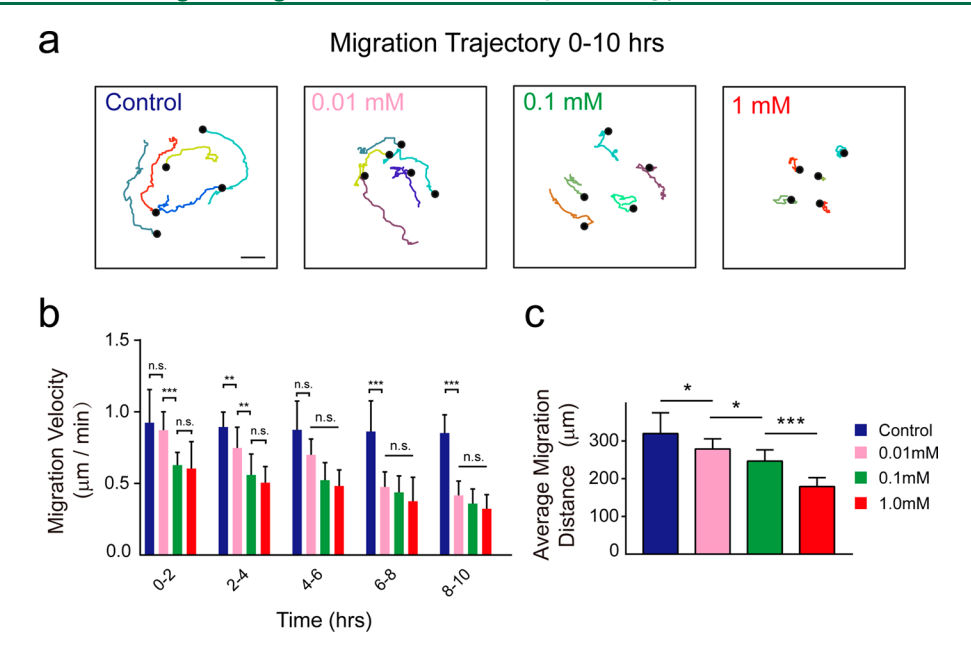


**Figure 5.** Cell migration speed and distance declined rapidly after lead exposure. (a) Migration trajectories of MDCK cells with or without lead treatment. Dots indicate the starting point, and lines indicate the trajectories. Scale bar,  $50 \mu m$ . (b) Bar plot presenting the cell migration average speed per 2 h from 0 to 10 h. (c) Bar plot showing the total cell migration distance from 0 to 10 h. n = 25 cells. MDCK cells were exposed to lead nitrate with 0, 0.01, 0.1, 1 mM for 2, 4, 6, 8, and 10 h. The migration velocity was analyzed at 2, 4, 6, 8, and 10 h, respectively. Data represent mean  $\pm$  standard deviation from at least three independent experiments. \*, P < 0.05, \*\*\*, P < 0.01, \*\*\*, P < 0.001, n.s., P > 0.05.

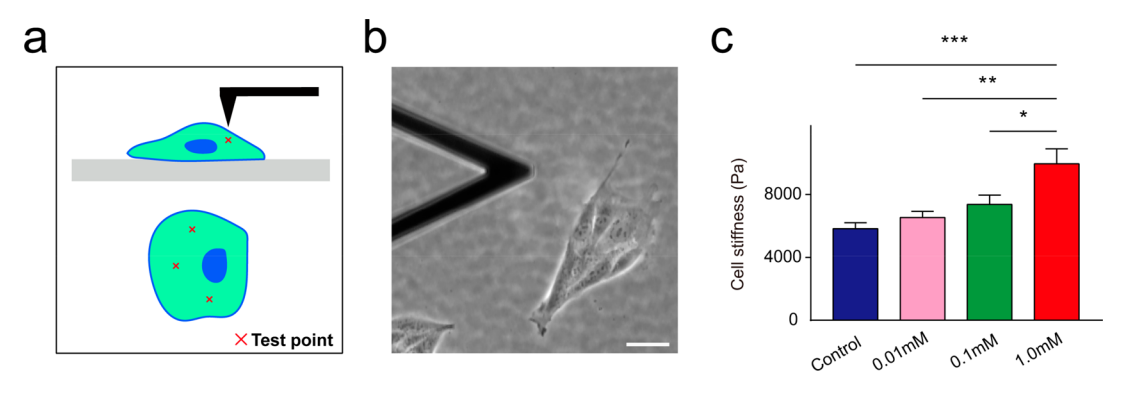


**Figure 6.** Cell stiffening after lead exposure as measured by AFM. (a) Schematic diagram showing the measurements on MDCK cells with AFM. Three positions away from the nuclear of one cell were selected and tested. (b) Representative phase image showing AFM probes and MDCK cells for measurement (c). MDCK cells were exposed to lead nitrate with 0, 0.01, 0.1, 1 mM for 24 h. Bar plot presenting the cell stiffness measured by AFM. Data represents mean  $\pm$  standard deviation from at least three independent experiments.  $n_{\text{cell}} = 31-33$  for each condition. \*, P < 0.05, \*\*\*, P < 0.01, \*\*\*, P < 0.001.

proteins.<sup>43</sup> It has been reported that lower cell mechanical stiffness favors cell motility, <sup>44</sup> and mechanical stiffness could be used as an indicator for the metastatic potential of cancer cells.<sup>7</sup> Thus, our results here are consistent with the observation that cell migration is attenuated in the lead-treated groups.

**Collective Cell Behaviors Change in Response to Lead.** In the previous section, we discussed the effects of pollutants on several biophysical properties at the single-cell level. As MDCK cells are well-established for the study epithelial functions, we investigated how lead disrupts the function of a monolayer of MDCK cells collectively, including permeability and wound closure speed. Although it has been reported that heavy metal exposure can lead to increased permeability and reduced wound closure speed, the sensitivity of those properties to lead at low concentrations remains unclear. 45,46 For the permeability measurement, we used a

standard transwell assay by seeding cells to form a confluent monolayer on a semipermeable membrane. After 24 h lead exposure, we added FITC-Dextran (40 000 wt) into the apical well and then recorded the fluorescence intensity of medium from the basolateral well (Figure 7a). Our results showed that while permeability increased drastically at a high lead concentration (1 mM), lower concentrations of lead only marginally induced permeability changes in cells (Figure 7b). To further elucidate differences in monolayer integrity between time points, a separate experiment was performed, where TEER was measured 2, 4, and 24 h after lead treatment (Figure S4). Our results confirmed the integrity of the MDCK monolayer prior to the lead treatment ( $\sim 500 \ \Omega \cdot \text{cm}^2$ ). More importantly, similar to the FITC-Dextran assay (Figure 7, 9), TEER measurements revealed that permeability changed rapidly (within 2 h) but only responded to a high dose of lead (1 mM).

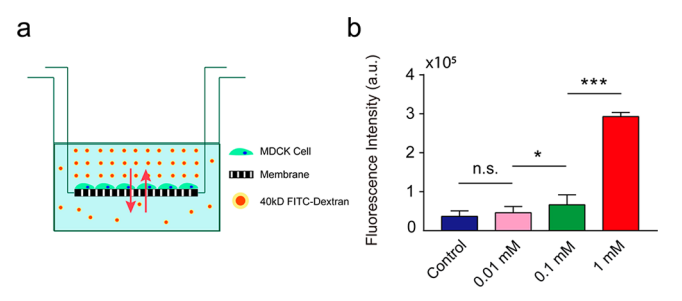


**Figure 7.** Monolayer permeability increased after lead exposure. (a) Schematic diagram showing the method of the transwell assay. (b) Bar plot indicating the absorbent fluorescence intensity of the medium absorbed from basolateral well. MDCK cells were exposed to lead nitrate with 0, 0.01, 0.1, 1 mM for 24 h. Data represent mean  $\pm$  standard deviation from at least three independent experiments. \*, P < 0.05, \*\*\*, P < 0.001, n.s., P > 0.05.

Another important function of epithelial cells is to maintain homeostasis when damaged. Both cell proliferation and collective migration contribute to the wound-healing process of epithelial cells. <sup>47–49</sup> We adopted a standard wound-healing assay to generate four wounds in a confluent monolayer of MDCK cells (Figure 8a), followed by lead treatment. Using

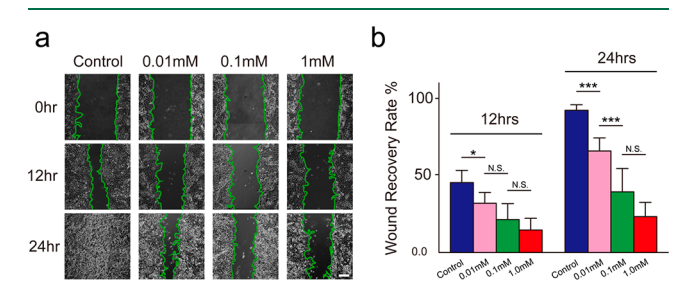


**Figure 8.** Effects of lead on cell wound healing. (a) Phase images showing the dynamics of wound-healing processes of MDCK cells treated with or without lead as indicated (eight images per condition). Scale bar, 300  $\mu$ m. (b) Bar plots showing the wound recovery rate after 12 and 24 h. MDCK cells were exposed to lead nitrate with 0, 0.01, 0.1, 1 mM for 24 h. Data represent mean  $\pm$  standard deviation from at least three independent experiments. \*, P < 0.05, \*\*\*, P < 0.001, n.s., P > 0.05.

time-lapse live-cell imaging, we monitored the wound-healing process continuously and analyzed the area of the wound over a 24 h period. Consistent with our previous findings of cell motility in the single-cell level, we found that the wound recovery extent, as determined by the recovered area divided by the original wound area, decreased from 45.3% (control, 12 h) and 92.3% (control, 24 h) to 32.0%, 21.4%, and 14.6% for 12 h, and 65.9%, 39.4%, and 23.3% for 24 h, after exposure to lead at 0.01, 0.1, 1.0 mM, respectively (Figure 8b).

The Rapid Change of Biophysical Properties in Response to Lead. So far we demonstrated that unlike conventional assays that could only detect dead cells, 50 biophysical properties could precisely detect subtle changes in cell physiology, especially at low concentrations. We next sought to determine the time sensitivity of various biophysical changes. MTT, LDH, permeability, and single-cell migration assays were performed at various time points after lead treatment to record the dynamic responses of cells. Results showed that within 4 h after lead exposure, there was no detectable alteration of cell viability as determined by the

MTT/LDH assays. In contrast, a drastic increase in cell permeability can be found in the 1 mM group, while lead at lower concentrations is insufficient to change cell permeability within this short period.

Moreover, single-cell migration speed appears to respond faster: within 2 h, a significant decrease could be detected at the concentration of 0.1 mM or higher, and this concentration limit could be further lowered to 0.01 mM in 4 h (Figure 9). Other properties require longer times to display any difference between control and treated group, and thus the results are not shown here. Together, single-cell migration speed and permeability were determined as the most time-sensitive methods for detecting cellular responses to lead.

The Pattern of Biophysical Features Changes in Responses to Cadmium. To understand the versatility of biophysical properties in assessing heavy metal toxicity, we tested another common toxicant, cadmium, on MDCK cells. First, an MTT assay was performed on MDCK cells treated with cadmium nitrate (hereinafter referred to as cadmium). Results showed that MDCK cell proliferation increased when treated with 0.005 and 0.05 mM of cadmium but decreased even lower than the control for the 0.5 mM treatment group (Figure S5a). Inversely, live-cell counting results show a dosedependent increase in cell death (Figure S5b), suggesting that cadmium may lead to increased cell proliferation as an adaptive response at lower concentrations and cytotoxicity at higher concentrations. This is consistent with previous findings that at a lower concentration, cadmium stimulates proliferation and DNA synthesis of various mammalian cells, 51-55 which potentially increases tumorigenic potential of cells. 56,57 As shown in Figure 10, the wound healing showed a similar trend as the MTT assay, suggesting that bulk assays could not distinguish the effect of cytotoxicity and proliferation at lower concentrations.

We then asked if single-cell assays such as traction force and focal adhesion analysis can better depict the cytotoxicity of cadmium. Interestingly, we found that the average traction forces per area (ATFs, Figure 11a, c) dramatically declined after 24 h treatment with a comparatively low concentration (0.005 mM) of cadmium. In addition, ATFs increased progressively with increasing concentration of cadmium. Results from focal adhesion investigation showed a similar trend as changes in traction forces (Figure 12). Notably, these results are in sharp contrast with those from the lead treatment, where both traction force and FA levels decrease with increasing lead concentrations. Together, these exciting results revealed that for cadmium, bulk cytotoxicity assays might be misleading in their assessments, as the potential damages to individual cells were masked by the increasing proliferation rate in those cytotoxicity assays and other bulk assays such as wound healing. Nevertheless, the single-cell assays might better reflect the toxicity of cadmium, as both traction forces and focal adhesions levels decreased with a very low concentration of cadmium treatment. It is interesting to observe that both traction forces and focal adhesion levels increase with the concentration of cadmium, in contrast to the lead treatment. These results reflect that the profile of a collection of biophysical features might be used to characterize the toxic mechanisms of different heavy metals.

REF Cells Experience Similar Biophysical Alterations When Exposed to Lead. We next aimed to determine whether lead-induced modifications of cellular biophysical properties are cell type dependent. Seeking a mesenchymal-like



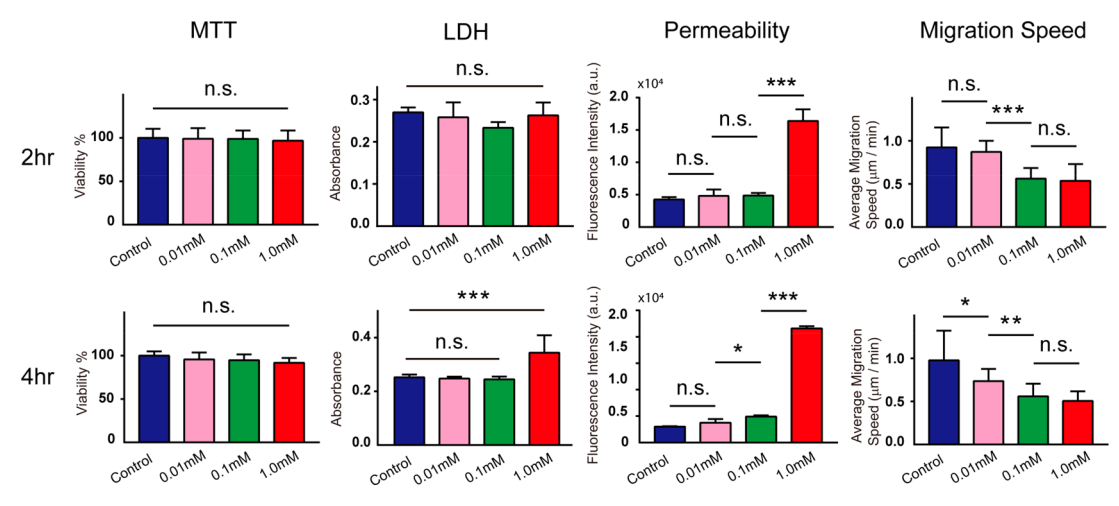


Figure 9. Rapid change of biophysical properties in response to lead. Bar plots showing the cell viability tested by (from left to right) the MTT assay, LDH assay, single layer cell permeability, and single cellular migration speed (right column) measured at the first 2 and 4 h. MDCK cells were exposed to lead nitrate with 0, 0.01, 0.1, 1 mM for 2 and 4 h. Data represent mean ± standard deviation from at least three independent experiments. \*, P < 0.05, \*\*, P < 0.01, \*\*\*, P < 0.001, n.s., P > 0.05.

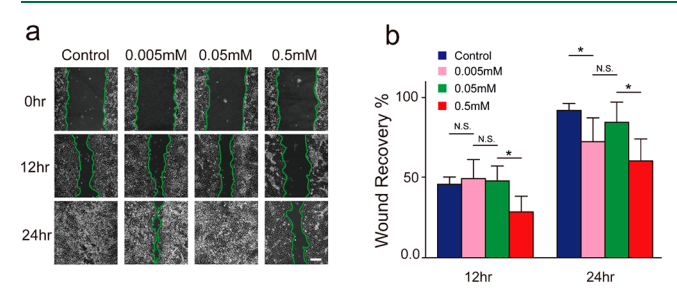


Figure 10. Effects of cadmium on cell wound healing. (a) Phase images showing the dynamics of wound-healing processes of MDCK cells treated with or without the cadmium as indicated (eight images per condition). Scale bar, 300  $\mu$ m. (b) Bar plots showing the wound recovery rate after 12 and 24 h. MDCK cells were exposed to cadmium nitrate with 0, 0.005, 0.05, 0.5 mM for 24 h. Data represent mean ± standard deviation from two independent experiments. \*, P < 0.05, n.s., P > 0.05.

cell with a strong contractile force to serve as a counterbalance for the epithelial-like MDCK cells, we performed experiments with REF cells. Regarding the LDH assay, REF cells were far more sensitive to lead than MDCK cells. REF cells had significantly greater absorbance readings in the 1 mM treatment group at all three time points (Figure S6). However, the absorbance values of the three lower concentrations (DI water, 0.01 and 0.1 mM) were indistinguishable as in the MDCK cell trials. After demonstrating that the LDH assay was equally ineffective in distinguishing the 0-0.1 mM treatment groups, we performed a cell migration assay and traction force analysis to determine the effects of lead on two biophysical traits of REF cells. Interestingly, despite fibroblasts' tendency for slow migration,<sup>58</sup> there was a noticeable change in the average migration distance and speed of REF cells. Though this difference is not as large as the MDCK, the difference between the DI water and 0.1 mM groups is statistically significant (Figure S7).4Traction force analysis on REF cells showed statistically significant changes in traction force per unit area for all four concentrations of lead (Figure S8). As fibroblasts are known to exert strong traction forces and migrate slowly, it is expected that changes of their biophysical

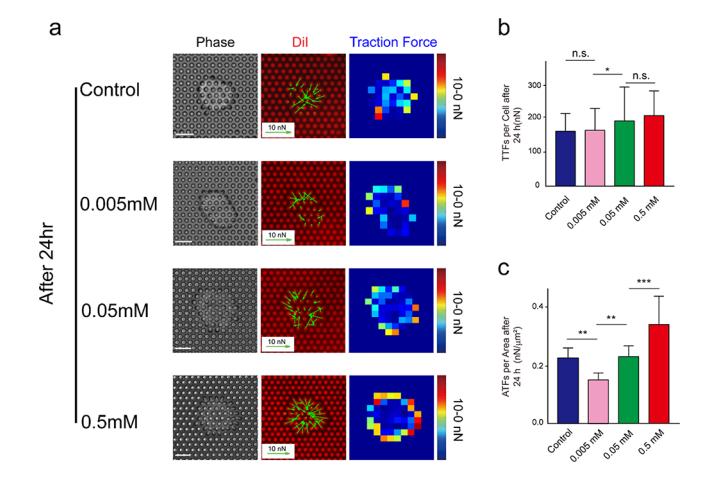
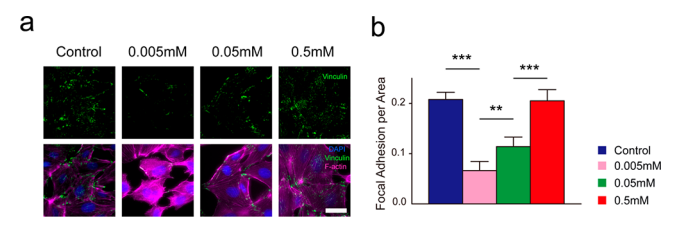


Figure 11. Cadmium induced a perturbation of cell traction forces. (a) Left: Representative phase images showing a MDCK cell exposed to cadmium on PMA substrates after 24 h. Middle: Microposts labeled with DiI (red) and vector maps of traction forces (green). Right: Colorimetric map showing traction forces. Scale bar, 10  $\mu$ m. (b-c) Bar plots comparing the TTFs (b) and ATFs (c) after 24 h. MDCK cells were exposed to cadmium nitrate with 0, 0.005, 0.05, 0.5 mM for 24 h. Data represents mean and standard deviation from two independent experiments. \*, P < 0.05, \*\*, P < 0.01, \*\*\*, P < 0.001, n.s., P > 0.05. n > 30 cells in each condition.

features in response to toxicants are different from MDCK

Correlations between Biophysical Phenotypes and **Lead Concentrations.** To determine the dynamic range of lead concentrations that can be distinguished by various detection methods, we used Pearson correlation coefficients (r) to evaluate the correlation between the lead concentration and cell viability or cell biophysical properties (Figure 13a). We found that for conventional cell viability assays, the modified live/dead assay presented a better negative correlation (r = -0.72) than the MTT assay (r = -0.53). In comparison, 6 out of 8 biophysical parameters we tested had r above 0.8. In particular, nuclear size (r = 0.93), cell stiffness (r = 0.93)= 0.96), and cell permeability (r = 0.99) are highly correlated with the lead concentration. It is interesting that traction force



**Figure 12.** Focal adhesions of MDCK cells disturbed after exposure to cadmium. (a) Representative immunofluorescence images showing focal adhesion distributions in MDCK cells for four experimental groups (control, 0.005, 0.05, and 0.5 mM). Scale bar, 25  $\mu$ m. (b) Bar plot presenting the area of focal adhesion per single cell. MDCK cells were exposed to cadmium nitrate with 0, 0.005, 0.05, 0.5 mM for 24 h. Data represent mean and standard deviation from two independent experiments. \*\*, P < 0.01, \*\*\*, P < 0.001. n > 30 cells in each condition.

changed the most significantly and earliest, while its correlation with lead doses was low. This might be due to the existence of basal level contractility in cells that could not decrease further or be accurately measured in our system. It is also possible that we detected a transient or adaptive response to lower concentrations. Furthermore, we combined the results in this study and generated a universal signature of cytotoxicity using both cell viability assays and biophysical parameters (Figure 13b). Although a single detection method might not be sensitive enough to depict cytotoxicity when exposed to lead, the combined approach can provide a fingerprint of cellular responses to toxicants at different concentrations. It is notable that although generally strong correlations between biophysical phenotypes and lead concentrations were in this study, more concentrations of lead need to be tested to establish a quantitative model to assess the severity of toxicity using these biophysical properties.

### DISCUSSION

Chronic kidney injury (CKI) caused by chronic exposure to low concentrations of toxicants has become a growing global health issue. While a variety of environmental factors, including lead and cadmium, have been implicated as potential causes of CKI, <sup>59</sup> it is still critical to identify possible environmental triggers of CKI. Our work showed that biophysical features may be used to sensitively identify cryptic renal toxicants. In addition, our findings that cytoskeleton structure rapidly changes after lead/cadmium treatment might also lead to new insights into the toxic mechanisms of heavy metals.

In this study, we systematically investigated how the biophysical properties of kidney epithelial cells change in response to lead, a common environmental toxicant. We found that compared with two conventional cell viability assays, biophysical properties were more sensitive and accurate for characterizing cellular responses to lead. In particular, traction force and FAs can be used to facilely identify cells exposed to a very low concentration of lead(II) nitrate (0.01 mM), while single-cell migration speed changes most quickly (within 2 h of lead exposure). Combining a panel of biophysical properties can adequately characterize the states of cells under different concentration of toxicants.

As an abundant heavy metal, lead has become one of the most notorious environmental toxicants derived from the widespread industrial application and faulty waste disposal. Current toxicological studies have demonstrated that lead exposure could induce oxidative stress, which was identified as the major adverse influence. Under the impact of lead, the ability of the cell to keep the balance between producing free radicals and detoxifying the reactive intermediate would be severely disturbed. Meanwhile, due to the ability of lead to substitute bivalent cations like Fe<sup>2+</sup>, Ca<sup>2+</sup>, and Mg<sup>2+</sup>, a variety of cellular and biological processes, including ionic trans-

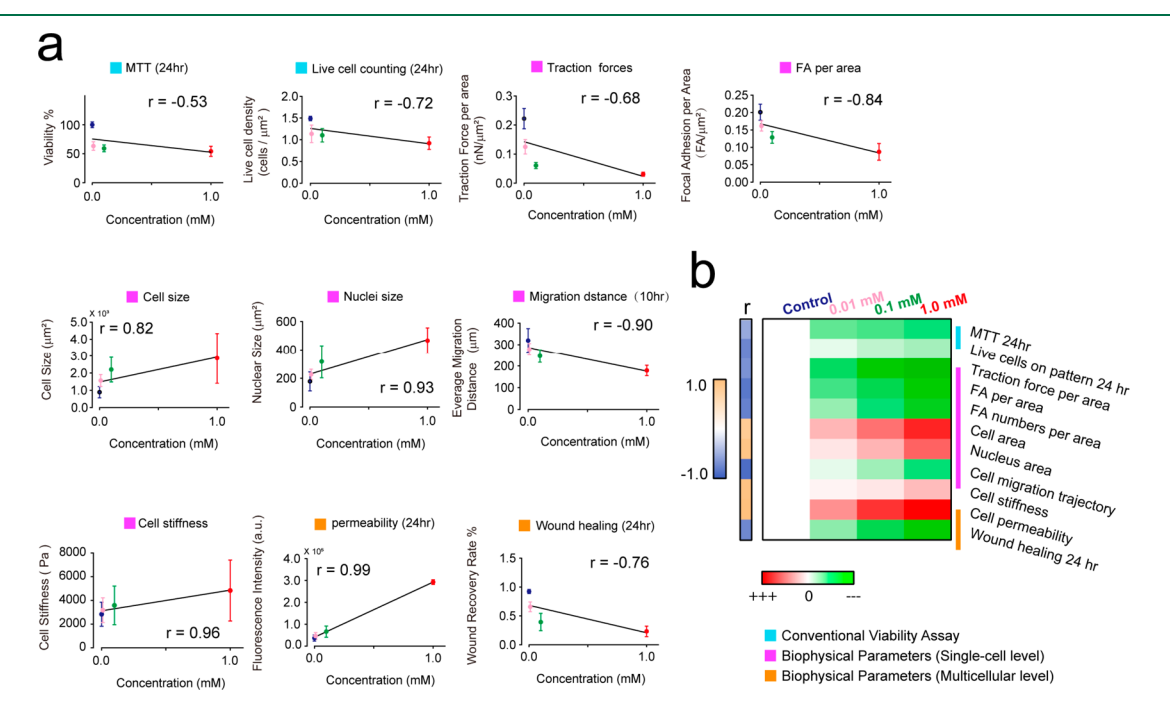


**Figure 13.** Strong correlations between biophysical phenotypes and lead concentrations. (a) Graphs showing the correlation between the concentration-associated variations of cell viability and biophysical parameters. r: Pearson correlation coefficients. (b) Colorimetric map indicating how lead alters cell viability and biophysical properties. Each column denotes an individual concentration-independent sample, and the left heatmap key denotes Pearson correlation coefficients. MDCK cells were exposed to lead nitrate with 0, 0.01, 0.1, 1 mM for 24 h.

portation, intra- and intercellular signaling, and the release of neurotransmitters, were disrupted. This substitution of lead for calcium might also explain the decreased permeability and contractility observed in our study, as Ca<sup>2+</sup> is required to maintain proper E-cadherins and cytoskeleton functions.

In normal physiological conditions, cell migration speed negatively correlates with traction forces, which positively correlate with cell and nuclear sizes. 26 However, our results demonstrated utterly different correlations between those biophysical properties when cells were exposed to lead. Cell migration speed decreased with increasing concentration of lead, while traction force also decreased, and the cell and nuclear area increased. This might be due to the stabilization of cytoskeleton by the lead, similar to the effects of divalent cations such as magnesium and calcium, which can cross-link actin and vimentin networks, resulting in a more stable and stiffer cytoskeleton.<sup>63</sup> Unstable FAs further inhibit cell migration. Also, swelling of the cells due to the alterations of osmotic pressure, cumulative substrate uptake, and oxidative stress<sup>64</sup> may directly contribute to cell and nuclear area changes, in addition to the effects of the cytoskeleton.

Our results suggest that the unique pattern of traction forces, cell migration, and cell shape may serve as a sensitive and robust hallmark of the cytotoxicity of heavy metals, as lead and cadmium led to very different patterns. Some biochemical methods such as measuring reactive oxygen species (ROS) or intracellular ATP are also sensitive for trace levels of toxicants; however, biophysical phenotyping might provide an alternative and potentially more sensitive way to identify toxicants and relative toxicities. Future works are needed to systematically establish the relationships between the concentration of various toxicants and biophysical features, expand the study to more cell types, and reveal the mechanism(s) for lead-related cytoskeleton dysfunctions, which is known to cause fibrotic remodeling in many organs. <sup>65</sup>

In summary, we quantitatively characterized lead-induced changes of several cell biophysical features, including traction forces, FAs, morphology, migration, stiffness, monolayer permeability, and wound-healing efficacy. These changes occurred at lower toxicant concentrations compared to the results of viability-based assays and thus have the potential to identify novel cell physiological changes to low concentrations of toxicants. We envision that biophysical phenotyping of cells may serve as a new screening tool for identifying cryptic toxicants. Moreover, our results suggest a new toxicological mechanism of environmental toxicants affecting the cytoskeleton structures in cells, which may lead to new therapeutic strategies for treating heavy metal poisoning. Importantly, while the biophysical changes we found are cause for toxicological concern, more studies are needed to understand whether they actually correspond to toxicity or an adverse event. Additionally, many assays performed in our work were based on single-cell analysis, without considering the intercellular physical interactions and paracrine signals. Future works are needed to reevaluate these results in the presence of neighboring cells.

## ASSOCIATED CONTENT

# Supporting Information

The Supporting Information is available free of charge at https://pubs.acs.org/doi/10.1021/acsbiomaterials.9b01640.

Schematic diagram showing the fabrication of PDMS micropost arrays (PMAs) and cell culture on PMAs, the LDH assay for characterizing MDCK cells viability, immunofluorescence images demonstrating lead-induced changes in both cellular and nuclear shape, bar plots showing lead-induced monolayer permeability changes, the live/dead assay and MTT assay for characterizing cadmium cytotoxicity, LDH assay for characterizing REF cells viability after lead exposure, REF cell migration speed and distance declining rapidly after lead exposure, and bar plots showing lead-induced reduction of cell traction forces of REF cells (PDF)

### AUTHOR INFORMATION

#### **Corresponding Authors**

Xiaofei Song — School of Environment and Energy, South China University of Technology, Guangzhou 510006, China; Email: songxf@scut.edu.cn

Yubing Sun — Department of Mechanical and Industrial Engineering and Department of Chemical Engineering, University of Massachusetts, Amherst, Massachusetts 01003, United States; ◎ orcid.org/0000-0002-6831-3383; Email: ybsun@umass.edu

#### **Authors**

Peiran Zhu — Department of Mechanical and Industrial Engineering, University of Massachusetts, Amherst, Massachusetts 01003, United States; Key Laboratory of 3D Micro/Nano Fabrication and Characterization of Zhejiang Province, School of Engineering, Westlake University, Hangzhou 310024, Zhejiang Province, China; Institute of Advanced Technology, Westlake Institute for Advanced Study, Hangzhou 310024, Zhejiang Province, China; Orcid.org/0000-0001-6007-6187

Jamar Hawkins — Department of Mechanical and Industrial Engineering, University of Massachusetts, Amherst, Massachusetts 01003, United States

Will Hamilton Linthicum — Department of Physics, Worcester Polytechnic Institute, Worcester, Massachusetts 01609, United States

Menglin Wang — Key Laboratory of 3D Micro/Nano Fabrication and Characterization of Zhejiang Province, School of Engineering, Westlake University, Hangzhou 310024, Zhejiang Province, China; Department of Chemistry and Chemical Engineering, Anhui University, Hefei 230601, Anhui Province, China

Ningwei Li — Department of Mechanical and Industrial Engineering, University of Massachusetts, Amherst, Massachusetts 01003, United States

Nanjia Zhou — Key Laboratory of 3D Micro/Nano Fabrication and Characterization of Zhejiang Province, School of Engineering, Westlake University, Hangzhou 310024, Zhejiang Province, China; Institute of Advanced Technology, Westlake Institute for Advanced Study, Hangzhou 310024, Zhejiang Province, China

Qi Wen – Department of Physics, Worcester Polytechnic Institute, Worcester, Massachusetts 01609, United States

Alicia Timme-Laragy — Department of Environmental Health Sciences, University of Massachusetts, Amherst, Massachusetts 01003, United States

Complete contact information is available at: https://pubs.acs.org/10.1021/acsbiomaterials.9b01640

#### **Author Contributions**

P.Z., J.H., X.S., and Y.S. designed experiments; P.Z., J.H., and W.H.L. performed experiments; N.L. analyzed the traction forces of cells; L.W.H. measured the cell stiffness by AFM; P.Z., M.W., Q.W., and Y.S. analyzed data; P.Z., N.L., W.H.L., N.Z., A.T., X.S., and Y.S. wrote the manuscript. All authors edited and approved the final manuscript.

## **Author Contributions**

These authors contribute equally to this work.

#### Notes

The authors declare no competing financial interest.

### ACKNOWLEDGMENTS

This work is supported in part by the National Science Foundation (CMMI 1662835 and CMMI 1846866 to Y.S.) and the Department of Mechanical and Industrial Engineering at the University of Massachusetts Amherst. The Conte Nanotechnology Cleanroom Lab is acknowledged for support in microfabrication.

# REFERENCES

- (1) Lee, W. C.; Shi, H.; Poon, Z.; Nyan, L. M.; Kaushik, T.; Shivashankar, G. V.; Chan, J. K.; Lim, C. T.; Han, J.; Van Vliet, K. J. Multivariate biophysical markers predictive of mesenchymal stromal cell multipotency. *Proc. Natl. Acad. Sci. U. S. A.* **2014**, *111* (42), E4409–18.
- (2) Settleman, J. Tension Precedes Commitment Even for a Stem Cell. *Mol. Cell* **2004**, *14* (2), 148–150.
- (3) Zhang, W.; Kai, K.; Ueno, N. T.; Qin, L. A Brief Review of the Biophysical Hallmarks of Metastatic Cancer Cells. *Cancer Hallmarkers* **2013**, *1* (2–3), 59–66.
- (4) Zhu, P.; Tseng, N.-H.; Xie, T.; Li, N.; Fitts-Sprague, I.; Peyton, S. R.; Sun, Y. Biomechanical Microenvironment Regulates Fusogenicity of Breast Cancer Cells. *ACS Biomater. Sci. Eng.* **2019**, *5* (8), 3817–3827.
- (5) Xue, X.; Sun, Y.; Resto-Irizarry, A. M.; Yuan, Y.; Aw Yong, K. M.; Zheng, Y.; Weng, S.; Shao, Y.; Chai, Y.; Studer, L.; Fu, J. Mechanics-guided embryonic patterning of neuroectoderm tissue from human pluripotent stem cells. *Nat. Mater.* **2018**, *17*, 633–641.
- (6) Swaminathan, V.; Mythreye, K.; O'Brien, E. T.; Berchuck, A.; Blobe, G. C.; Superfine, R. Mechanical stiffness grades metastatic potential in patient tumor cells and in cancer cell lines. *Cancer Res.* **2011**, 71 (15), 5075–80.
- (7) Xu, W.; Mezencev, R.; Kim, B.; Wang, L.; McDonald, J.; Sulchek, T. Cell Stiffness Is a Biomarker of the Metastatic Potential of Ovarian Cancer Cells. *PLoS One* **2012**, *7* (10), e46609.
- (8) Phillip, J. M.; Wu, P.-H.; Gilkes, D. M.; Williams, W.; McGovern, S.; Daya, J.; Chen, J.; Aifuwa, I.; Lee, J. S. H.; Fan, R.; Walston, J.; Wirtz, D. Biophysical and biomolecular determination of cellular age in humans. *Nat. Biomed. Eng.* **2017**, *1*, 0093.
- (9) Gossett, D. R.; Tse, H. T.; Lee, S. A.; Ying, Y.; Lindgren, A. G.; Yang, O. O.; Rao, J.; Clark, A. T.; Di Carlo, D. Hydrodynamic stretching of single cells for large population mechanical phenotyping. *Proc. Natl. Acad. Sci. U. S. A.* **2012**, *109* (20), 7630–5.
- (10) Barbier, O.; Jacquillet, G.; Tauc, M.; Cougnon, M.; Poujeol, P. Effect of Heavy Metals on, and Handling by, the Kidney. *Nephron Physiology* **2005**, *99* (4), p105–p110.
- (11) Fowler, B. A.; DuVal, G. Effects of lead on the kidney: roles of high-affinity lead-binding proteins. *Environ. Health Perspect.* **1991**, *91*, 77–80.
- (12) Ingber, D. E. Mechanobiology and diseases of mechanotransduction. *Ann. Med.* **2003**, 35 (8), 564–77.
- (13) Coresh, J.; Astor, B. C.; Greene, T.; Eknoyan, G.; Levey, A. S. Prevalence of chronic kidney disease and decreased kidney function in the adult US population: Third National Health and Nutrition Examination Survey. *Am. J. Kidney Dis.* **2003**, *41* (1), 1–12.

- (14) Milicevic, D. R.; Jovanovic, M.; Juric, V. B.; Petrovic, Z. I.; Stefanovic, S. M. Toxicological assessment of toxic element residues in swine kidney and its role in public health risk assessment. *Int. J. Environ. Res. Public Health* **2009**, *6* (12), 3127–42.
- (15) Seidl, K.; Zinkernagel, A. S. The MTT assay is a rapid and reliable quantitative method to assess Staphylococcus aureus induced endothelial cell damage. *J. Microbiol. Methods* **2013**, 92 (3), 307–309.
- (16) Wei, Z. X.; Shaikh, Z. A. Cadmium stimulates metastasis-associated phenotype in triple-negative breast cancer cells through integrin and beta-catenin signaling. *Toxicol. Appl. Pharmacol.* **2017**, 328, 70–80.
- (17) Khan, H.; Singh, R. D.; Tiwari, R.; Gangopadhyay, S.; Roy, S. K.; Singh, D.; Srivastava, V. Mercury exposure induces cytoskeleton disruption and loss of renal function through epigenetic modulation of MMP9 expression. *Toxicology* **2017**, *386*, 28–39.
- (18) Egbowon, B. F.; Harris, W.; Arnott, G.; Mills, C. L.; Hargreaves, A. J. Sub-lethal concentrations of CdCl2 disrupt cell migration and cytoskeletal proteins in cultured mouse TM4 Sertoli cells. *Toxicol. In Vitro* **2016**, *32*, 154–165.
- (19) Soenen, S. J.; Manshian, B.; Montenegro, J. M.; Amin, F.; Meermann, B.; Thiron, T.; Cornelissen, M.; Vanhaecke, F.; Doak, S.; Parak, W. J.; De Smedt, S.; Braeckmans, K. Cytotoxic Effects of Gold Nanoparticles: A Multiparametric Study. *ACS Nano* **2012**, *6* (7), 5767–5783.
- (20) Koeneman, B. A.; Zhang, Y.; Westerhoff, P.; Chen, Y. S.; Crittenden, J. C.; Capco, D. G. Toxicity and cellular responses of intestinal cells exposed to titanium dioxide. *Cell Biol. Toxicol.* **2010**, 26 (3), 225–238.
- (21) Coradeghini, R.; Gioria, S.; Garcia, C. P.; Nativo, P.; Franchini, F.; Gilliland, D.; Ponti, J.; Rossi, F. Size-dependent toxicity and cell interaction mechanisms of gold nanoparticles on mouse fibroblasts. *Toxicol. Lett.* **2013**, *217* (3), 205–216.
- (22) Tchounwou, P. B.; Yedjou, C. G.; Foxx, D. N.; Ishaque, A. B.; Shen, E. Lead-induced cytotoxicity and transcriptional activation of stress genes in human liver carcinoma (HepG2) cells. *Mol. Cell. Biochem.* **2004**, 255 (1–2), 161–70.
- (23) Yedjou, C. G.; Tchounwou, P. B. Lead-Induced Cell Cycle Arrest in Human Liver Carcinoma (HepG(2)) Cells: Involvement of Oxidative Stress, p53 and Cyclin A. *Met Ions Biol.* **2011**, *11*, 242–246.
- (24) Denizot, F.; Lang, R. Rapid colorimetric assay for cell growth and survival: Modifications to the tetrazolium dye procedure giving improved sensitivity and reliability. *J. Immunol. Methods* **1986**, 89 (2), 271–277.
- (25) Lam, R. H. W.; Sun, Y. B.; Chen, W. Q.; Fu, J. P. Elastomeric microposts integrated into microfluidics for flow-mediated endothelial mechanotransduction analysis. *Lab Chip* **2012**, *12* (10), 1865–1873.
- (26) Fu, J. P.; Wang, Y. K.; Yang, M. T.; Desai, R. A.; Yu, X. A.; Liu, Z. J.; Chen, C. S. Mechanical regulation of cell function with geometrically modulated elastomeric substrates. *Nat. Methods* **2010**, *7* (9), 733–736.
- (27) Weng, S.; Shao, Y.; Chen, W.; Fu, J. Mechanosensitive subcellular rheostasis drives emergent single-cell mechanical homeostasis. *Nat. Mater.* **2016**, *15*, 961.
- (28) Piccinini, F.; Kiss, A.; Horvath, P. CellTracker (not only) for dummies. *Bioinformatics* **2016**, 32 (6), 955–7.
- (29) Thomas, G.; Burnham, N. A.; Camesano, T. A.; Wen, Q. Measuring the Mechanical Properties of Living Cells Using Atomic Force Microscopy. *J. Visualized Exp.* **2013**, No. 76, e50497.
- (30) Hertz, H. Ueber die Berührung fester elastischer Körper. Journal für die reine und angewandte Mathematik (Crelle's Journal) 1882, 1882, 156.
- (31) Morcillo, P.; Esteban, M. Á.; Cuesta, A. Heavy metals produce toxicity, oxidative stress and apoptosis in the marine teleost fish SAF-1 cell line. *Chemosphere* **2016**, *144*, 225–233.
- (32) Berridge, M. V.; Herst, P. M.; Tan, A. S., Tetrazolium dyes as tools in cell biology: New insights into their cellular reduction. In *Biotechnology Annual Review*; Elsevier: Amsterdam, Netherlands, 2005; Vol. 11, pp 127–152.

- (33) Jo, H. Y.; Kim, Y.; Park, H. W.; Moon, H. E.; Bae, S.; Kim, J.; Kim, D. G.; Paek, S. H. The Unreliability of MTT Assay in the Cytotoxic Test of Primary Cultured Glioblastoma Cells. *Exp Neurobiol* **2015**, 24 (3), 235–45.
- (34) Ingber, D. E. Cellular mechanotransduction: putting all the pieces together again. FASEB J. 2006, 20 (7), 811–827.
- (35) Munevar, S.; Wang, Y.; Dembo, M. Traction force microscopy of migrating normal and H-ras transformed 3T3 fibroblasts. *Biophys. J.* **2001**, *80* (4), 1744–57.
- (36) Sun, Y.; Chen, C. S.; Fu, J. Forcing stem cells to behave: a biophysical perspective of the cellular microenvironment. *Annu. Rev. Biophys.* **2012**, *41*, 519–42.
- (37) Sun, Y.; Villa-Diaz, L. G.; Lam, R. H.; Chen, W.; Krebsbach, P. H.; Fu, J. Mechanics regulates fate decisions of human embryonic stem cells. *PLoS One* **2012**, *7* (5), e37178.
- (38) Dumbauld, D. W.; Lee, T. T.; Singh, A.; Scrimgeour, J.; Gersbach, C. A.; Zamir, E. A.; Fu, J.; Chen, C. S.; Curtis, J. E.; Craig, S. W.; García, A. J. How vinculin regulates force transmission. *Proc. Natl. Acad. Sci. U. S. A.* **2013**, *110* (24), 9788–9793.
- (39) Volland, S.; Bayer, E.; Baumgartner, V.; Andosch, A.; Lutz, C.; Sima, E.; Lutz-Meindl, U. Rescue of heavy metal effects on cell physiology of the algal model system Micrasterias by divalent ions. *J. Plant Physiol.* **2014**, *171* (2), 154–63.
- (40) Chen, C. S.; Mrksich, M.; Huang, S.; Whitesides, G. M.; Ingber, D. E. Micropatterned surfaces for control of cell shape, position, and function. *Biotechnol. Prog.* **1998**, *14* (3), 356–363.
- (41) Martin, P. Wound Healing-Aiming for Perfect Skin Regeneration. Science 1997, 276 (5309), 75-81.
- (42) Discher, D. E.; Janmey, P.; Wang, Y.-l. Tissue cells feel and respond to the stiffness of their substrate. *Science* **2005**, *310* (5751), 1139–1143.
- (43) Wagner, O. I.; Rammensee, S.; Korde, N.; Wen, Q.; Leterrier, J. F.; Janmey, P. A. Softness, strength and self-repair in intermediate filament networks. *Exp. Cell Res.* **2007**, 313 (10), 2228–35.
- (44) Luo, Q.; Kuang, D.; Zhang, B.; Song, G. Cell stiffness determined by atomic force microscopy and its correlation with cell motility. *Biochim. Biophys. Acta, Gen. Subj.* **2016**, *1860* (9), 1953–60.
- (45) Salton, M. R. Lytic agents, cell permeability, and monolayer penetrability. J. Gen. Physiol. 1968, 52 (1), 227–52.
- (46) Chen, C.-T.; Chen, T.-H.; Lo, K.-F.; Chiu, C.-Y. Effects of proline on copper transport in rice seedlings under excess copper stress. *Plant Sci.* **2004**, *166* (1), 103–111.
- (47) Suresh, S. Biomechanics and biophysics of cancer cells. *Acta Biomater.* **2007**, 3 (4), 413–438.
- (48) Yue, H.; Yun, Y.; Gao, R.; Li, G.; Sang, N. Winter Polycyclic Aromatic Hydrocarbon-Bound Particulate Matter from Peri-urban North China Promotes Lung Cancer Cell Metastasis. *Environ. Sci. Technol.* **2015**, *49* (24), 14484–93.
- (49) Farooqui, R.; Fenteany, G. Multiple rows of cells behind an epithelial wound edge extend cryptic lamellipodia to collectively drive cell-sheet movement. *J. Cell Sci.* **2005**, *118*, 51–63.
- (50) Ferguson, M. A.; Vaidya, V. S.; Bonventre, J. V. Biomarkers of nephrotoxic acute kidney injury. *Toxicology* **2008**, *245* (3), 182–93.
- (51) Jiang, G.; Duan, W.; Xu, L.; Song, S.; Zhu, C.; Wu, L. Biphasic effect of cadmium on cell proliferation in human embryo lung fibroblast cells and its molecular mechanism. *Toxicol. In Vitro* **2009**, 23 (6), 973–8.
- (52) von Zglinicki, T.; Edwall, C.; Ostlund, E.; Lind, B.; Nordberg, M.; Ringertz, N. R.; Wroblewski, J. Very low cadmium concentrations stimulate DNA synthesis and cell growth. *J. Cell Sci.* **1992**, *103* (4), 1073–1081.
- (53) Ronchetti, S. A.; Miler, E. A.; Duvilanski, B. H.; Cabilla, J. P. Cadmium Mimics Estrogen-Driven Cell Proliferation and Prolactin Secretion from Anterior Pituitary Cells. *PLoS One* **2013**, *8* (11), e81101.
- (54) Wang, B.; Ji, K.; Wang, Y.; Li, Y.; Tang, Y.; Gu, J.; Cai, L. Exposure to low dose cadmium enhances FL83B cells proliferation through down-regulation of caspase-8 by DNA hypermethylation. *Toxicol. Res.* **2015**, *4* (2), 248–259.

- (55) Fujiwara, Y.; Watanabe, S.; Kaji, T. Promotion of cultured vascular smooth muscle cell proliferation by low levels of cadmium. *Toxicol. Lett.* **1998**, *94* (3), 175–80.
- (56) Chen, Y. Y.; Zhu, J. Y.; Chan, K. M. Effects of cadmium on cell proliferation, apoptosis, and proto-oncogene expression in zebrafish liver cells. *Aquat. Toxicol.* **2014**, *157*, 196–206.
- (57) Bloomfield, M.; Louie, M. C. Chronic cadmium exposure decreases the dependency of MCF7 breast cancer cells on ERalpha. *Sci. Rep.* **2019**, *9* (1), 12135.
- (58) Trepat, X.; Chen, Z.; Jacobson, K. Cell migration. Compr. Physiol. 2012, 2 (4), 2369-92.
- (59) Obrador, G. T.; Schultheiss, U. T.; Kretzler, M.; Langham, R. G.; Nangaku, M.; Pecoits-Filho, R.; Pollock, C.; Rossert, J.; Correa-Rotter, R.; Stenvinkel, P.; Walker, R.; Yang, C. W.; Fox, C. S.; Kottgen, A. Genetic and environmental risk factors for chronic kidney disease. *Kidney Int. Suppl.* **2017**, *7* (2), 88–106.
- (60) Verstraeten, S. V.; Aimo, L.; Oteiza, P. I. Aluminium and lead: molecular mechanisms of brain toxicity. *Arch. Toxicol.* **2008**, 82 (11), 789–802.
- (61) Patra, R. C.; Rautray, A. K.; Swarup, D. Oxidative stress in lead and cadmium toxicity and its amelioration. *Vet. Med. Int.* **2011**, 2011, 457327.
- (62) Chatterjee, S.; Sarkar, S.; Bhattacharya, S. Toxic metals and autophagy. Chem. Res. Toxicol. 2014, 27 (11), 1887–900.
- (63) Huisman, E. M.; Wen, Q.; Wang, Y. H.; Cruz, K.; Kitenbergs, G.; Erglis, K.; Zeltins, A.; Cebers, A.; Janmey, P. A. Gelation of semiflexible polyelectrolytes by multivalent counterions. *Soft Matter* **2011**, 7 (16), 7257–7261.
- (64) Schliess, F.; Schreiber, R.; Häussinger, D. Activation of extracellular signal-regulated kinases Erk-1 and Erk-2 by cell swelling in H4IIE hepatoma cells. *Biochem. J.* **1995**, *309*, 13–17.
- (65) Tschumperlin, D. J.; Ligresti, G.; Hilscher, M. B.; Shah, V. H. Mechanosensing and fibrosis. *J. Clin. Invest.* **2018**, *128* (1), 74–84.